Journal Pre-proofs

Full Length Article

Insight into the promotional mechanism of Cu modification towards wide-temperature NH_3-SCR performance of NbCe catalyst

Dongqi An, Yuyao Yang, Weixin Zou, Yandi Cai, Qing Tong, Jingfang Sun, Lin Dong

PII: S1004-9541(22)00247-6
DOI: https://doi.org/10.1016/j.cjche.2022.05.028
Reference: CJCHE 2693

To appear in: *Chinese Journal of Chemical Engineering*

Received Date: 20 March 2022
Revised Date: 19 May 2022
Accepted Date: 24 May 2022

Please cite this article as: D. An, Y. Yang, W. Zou, Y. Cai, Q. Tong, J. Sun, L. Dong, Insight into the promotional mechanism of Cu modification towards wide-temperature NH_3-SCR performance of NbCe catalyst, *Chinese Journal of Chemical Engineering* (2022), doi: https://doi.org/10.1016/j.cjche.2022.05.028

Full Length Article

Insight into the promotional mechanism of Cu modification towards wide-temperature NH_3-SCR performance of NbCe catalyst

Dongqi An[1], Yuyao Yang[2], Weixin Zou[3], Yandi Cai[3], Qing Tong[4], Jingfang Sun[4,*], Lin Dong[5,*]

[1] Key Laboratory of Mesoscopic Chemistry of MOE, School of Chemistry and Chemical Engineering and Jiangsu Key Laboratory of Vehicle Emissions Control, Nanjing University, Nanjing 210093, China

[2] Center for Nanochemistry, College of Chemistry and Molecular Engineering, Peking University, Beijing 100871, China

[3] Jiangsu Key Laboratory of Vehicle Emissions Control, School of Environment, Nanjing University, Nanjing 210093, China

[4] Jiangsu Key Laboratory of Vehicle Emissions Control, Center of Modern Analysis, Nanjing University, Nanjing 210093, China

[5] Key Laboratory of Mesoscopic Chemistry of MOE, School of Chemistry and Chemical Engineering and Jiangsu Key Laboratory of Vehicle Emissions Control, School of Environment, Center of Modern Analysis, Nanjing University, Nanjing 210093, China

*Corresponding Authors

E-mail: sunjf@nju.edu.cn; donglin@nju.edu.cn

Abstract

A simple strategy of Cu modification was proposed to broaden the operation temperature window for NbCe catalyst. The best catalyst $Cu_{0.010}/Nb_1Ce_3$ presented over

90% NO conversion in a wide temperature range of 200−400 °C and exhibited an excellent H_2O or/and SO_2 resistance at 275 °C. To understand the promotional mechanism of Cu modification, the correlation among the "activity-structure-property" were tried to establish systematically. Cu species highly dispersed on NbCe catalyst to serve as the active component. The strong interaction among Cu, Nb and Ce promoted the emergence of NbO_4 and induced more Brønsted acid sites. And Cu modification obviously enhanced the redox behavior of the NbCe catalyst. Besides, EPR probed the Cu species exited in the form of monomeric and dimeric Cu^{2+}, the isolated Cu^{2+} acted as catalytic active sites to promote the reaction: Cu^{2+}-NO_3^-+NO(g) → Cu^{2+}-NO_2^- +NO_2(g). Then the generated NO_2 would accelerate the fast-SCR reaction process and thus facilitated the low-temperature deNO_x efficiency. Moreover, surface nitrates became unstable and easy to decompose after Cu modification, thus providing additional adsorption and activation sites for NH_3, and ensuring the improvement of catalytic activity at high temperature. Since the NH_3-SCR reaction followed by E-R reaction pathway efficaciously over $Cu_{0.010}/Nb_1Ce_3$ catalyst, the excellent H_2O and SO_2 resistance was as expected.

Keywords: NH_3-SCR, NbCe catalyst, Cu modification, NO_2 promoting effect, fast-SCR, flue gas

Graphical abstract

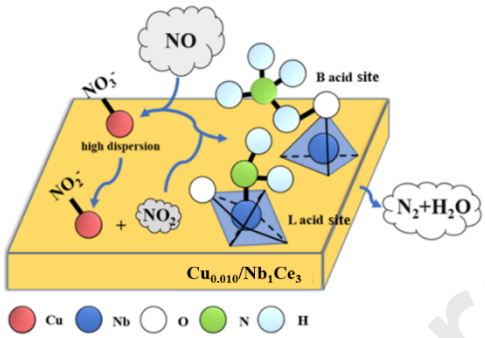

1. Introduction

The abatement of nitrogen oxides (NO_x), one of the main contributors of atmospheric pollution, is still a challenging task worldwide [1-4]. Among the denitrification techniques developed in recent years, NH_3-SCR has been adopted as the most promising and commercial employed procedure for NO_x removal from stationary boilers and coal-fired plants [5, 6]. And the TiO_2-anatase supported V_2O_5-WO_3 or V_2O_5-MoO_3 oxides have been commercialized for flue gas (300−400 °C) emitted from abovementioned stationary applications. Nevertheless, there are still some shortcomings, such as the biological toxicity of V_2O_5 to human and eco-environment, narrow operation temperature window, and unselective oxidation of NH_3 to N_2O, which constrain their application for nonelectric plant [7-9]. Therefore, it is compulsory to develop environmental-friendly NH_3-SCR catalysts with exceptional low-temperature NO conversion, high N_2 selectivity and a broad operating temperature window as

alternatives.

Some transition metal oxides, such as MnO_x, CuO, Fe_2O_3 and CeO_2 have been found to be active for the SCR of NO with NH_3 [10-13]. Among them, CeO_2 has been extensively investigated due to (i) the excellent oxygen storage capacities (OSC) on the basis of the redox behavior between Ce^{3+} and Ce^{4+}; (ii) the relatively easy formation of labile oxygen vacancies and the high mobility of bulk oxygen species [14]. Besides, the acid site and redox site are always highly valued in the NH_3-SCR process [15], so it's found that modifying CeO_2-based materials with acidic metal oxides (WO_3, Nb_2O_5 and MoO_3 as examples) could dramatically promote their SCR performance [6, 16-18]. Among them, the Nb_2O_5-CeO_2 catalyst system was proven to show great potential for diesel NO_x emission control due to adequate activity and high thermal stability [19]. However, NbCe catalysts with desirable NO_x elimination performance at a broad operation temperature window are still in urgent need, and the poisoning tolerance to water vapor and sulfur oxides ubiquitously found in flue gas also waited to be enhanced [20]. The commonly reported Cu were widely used as active species, which exhibited superior low-temperature NH_3-SCR activity. As reported in the literature, the redox capacity of CeO_2 could be promoted drastically by Cu modification [21-23]. And numerous studies manifested that the surface area, redox behavior and reactivity of NH_3 together with absorbed nitrate were notably elevated for the binary Cu and Nb oxides [24-26].

In this work, Cu was adopted as active species to modify NbCe catalyst and the

optimal molar ratio of Cu/NbCe was explored. Then the promotional mechanism of Cu modification was comprehensively elucidated through clarifying the relationship among the "activity - structure - property" in depth.

2. Materials and Methods

2.1 Catalyst preparation

NbCe binary oxides were prepared by co-precipitation method. Desired amount of $C_{10}H_5NbO_{20}$ and $Ce(NO_3)_3 \cdot 6H_2O$ was adequately dissolved in deionized water, ammonia solution was then added dropwise to the mixture with continuous stirring until pH = 10. The mixture was further stirred for 3 h and then aged for 1 h. Afterwards, the precipitates were collected by filtration for several times and dried at 100 ^oC overnight and calcined at 500 ^oC for 4 h under air conditions. The catalysts were crushed and sieved to 40-60 meshes for activity tests. The molar ratios of Nb/Ce were 1/3, 1/1 and 3/1. The obtained catalysts were denoted as Nb_1Ce_3, Nb_1Ce_1 and Nb_3Ce_1.

Cu/NbCe ternary oxides were prepared by impregnation method. Desired amount of $Cu(NO_3)_2 \cdot 6H_2O$ and the prepared NbCe powders were adequately dissolved in deionized water. The mixture was sufficiently stirred and heated at 80 °C until water was evaporated and a porous gel was formed. The gel was dried at 100 °C overnight and calcined at 500 ^oC for 4 h under air conditions. The catalysts were crushed and sieved to 40-60 meshes for activity tests. The obtained catalysts were denoted as $Cu_{0.005}/Nb_1Ce_3$, $Cu_{0.010}/Nb_1Ce_3$ and $Cu_{0.030}/Nb_1Ce_3$ (molar ratio).

2.2 Characterization

X-ray diffraction (XRD) patterns were recorded on a Philips X'pert Pro diffractometer using Ni-filtered Cu K_α radiation (λ = 0.15418 nm) from 10° to 80°. The X-ray tube was operated at 40 kV and 30 mA.

X-ray fluorescence (XRF) measurements were performed on a ARL9800XP+ spectrometer to quantify the actual Cu contents of the samples.

N_2 adsorption-desorption measurements were performed at −196 °C using a Micromeritics ASAP-3020 analyzer. All samples were firstly degassed in vacuum at 300 °C. The specific surface areas of samples were calculated via Brunauer-Emmett-Teller (BET) method.

Laser Raman spectra were collected on a LabRAM Aramis (Japan Horiba) Laser Raman spectrometer with an Ar^+ laser beam with an emission line at 532 nm. The laser power was 10 mW.

X-ray Photoelectron Spectroscopy (XPS) experiments were performed on a PHI 5000 Versa Probe system equipped with a monochromatic Al X-ray radiation source (1486.6 eV) with an accelerating power of 15 kW. Binding energies (BE) of all the elements were calibrated with C1s at 284.6 eV.

H_2-temperature-programed reduction (H_2-TPR) was performed in a quartz U-tube reactor connected to a thermal conductivity detector (TCD). An H_2-Ar (7% H_2) mixture was used as reductant. The 10 mg samples were pretreated with purified N_2 at 200 °C for 1 h. The range of measuring temperature was 20 °C to 800 °C at a rate of 10 °C·min^{-1}.

Electron paramagnetic resonance (EPR) spectra were recorded by a Bruker EMX

spectrometer using 100 kHz modulation and 4-G standard modulation width.

Temperature programmed desorption (TPD) measurements were carried out in a fixed-bed quartz reactor equipped with a FTIR spectrometer to monitor outlet gas signal and the interval of spectrum collecting was set at 30 s. For NH_3/NO_2-TPD experiment: the 100 mg samples were exposed to 0.5‰ NH_3 or 0.5‰ NO_2 (gas mixture of 50 ml·min^{-1}, Ar balanced) until saturation at ambient temperature. Subsequently, purged the samples with the flowing high purified Ar to remove gaseous and weakly absorbed species. Finally, the samples were heated to 500/400 ^{o}C at a rate of 10 ^{o}C·min^{-1} to record the NH_3 or NO_2 signal.

in situ DRIFTS experiments were conducted on a Nicolet Nexus 5700 FTIR spectrometer. The spectra were collected by an MCT detector and presented as a Kubelka-Munk function. The resolution was 4 cm^{-1} and 32 scans were taken. Before collecting the background spectra, the powder samples were pretreated with high purified N_2 at 400 ^{o}C. Background spectra were then collected in a flowing high purified N_2 stream as the powder samples cooled to each desired temperature. The sample spectra were then obtained after the subtraction of the background spectra at each desired temperature. The samples were exposed to a controlled stream of specific gas mixture for a certain amount of time: 3‰ NH_3; 3‰ NO + 5 %(volume) O_2. All of the reaction gasses were balanced with N_2 at a flow rate of 50 ml·min^{-1}.

2.3 SCR performance measurements

The NH_3-SCR activity and N_2 selectivity on the as-prepared samples were

measured in a fixed-bed quartz flow reactor with 200 mg of catalyst. The feed gases were composed of 0.5‰ NO, 0.5‰ NH_3, 5 %(volume) O_2, 0.2‰ SO_2 (when used), 5 %(volume) H_2O (when used) and balanced with Ar. The total flow rate was 200 $ml \cdot min^{-1}$ and the WHSV (weight hourly space velocity) was 60,000 $ml \cdot g^{-1} \cdot h^{-1}$. Before starting the activity test, the catalysts were pretreated in Ar at 200 °C for 1 h. The outlet gas concentrations were measured by an online Thermofisher IS10 FTIR spectrometer. The NO conversion and N_2 selectivity of the NH_3-SCR reaction were determined according to the following equations:

$$\text{NO conversion} = \frac{[NO]_{in} - [NO]_{out}}{[NO]_{in}} \times 100\% \quad (1)$$

$$N_2 \text{ selectivity} = \frac{[NO]_{in} - [NO]_{out} + [NH_3]_{in} - [NH_3]_{out} - [NO_2]_{out} - 2[N_2O]_{out}}{[NO]_{in} - [NO]_{out} + [NH_3]_{in} - [NH_3]_{out}} \times 100\% \quad (2)$$

3. Results and Discussion

3.1 Catalytic performance

The NO conversion and N_2 selectivity over Nb_1Ce_3, Nb_1Ce_1 and Nb_3Ce_1 were evaluated in broad temperature of 100 °C to 400 °C, and the corresponding results were shown in Fig. 1(a-b). All the NbCe catalysts had the favorable N_2 selectivity and the Nb_1Ce_3 catalyst displayed the best NO removal efficiency in the range of 100 °C to 400 °C, so it was adopted as the support in the following study. Then the catalytic performance over $Cu_{0.005}/Nb_1Ce_3$, $Cu_{0.010}/Nb_1Ce_3$ and $Cu_{0.030}/Nb_1Ce_3$ were reported in Fig. 1(c-d). It could be clearly seen that the Cu modification efficaciously enhanced the denitration efficiency and N_2 selectivity in a wide temperature. As the Cu adding amount increased, the NH_3-SCR activity on Cu/Nb_1Ce_3 catalysts initially increased and

then decreased. $Cu_{0.010}/Nb_1Ce_3$ performed the supreme NH_3-SCR activity in the entire temperature range, over which exceeding 90% NO conversion was accomplished from 200 °C to 400 °C. It was concluded that the proper amount of Cu modification significantly boosted the $DeNO_x$ efficiency of Nb_1Ce_3 catalyst.

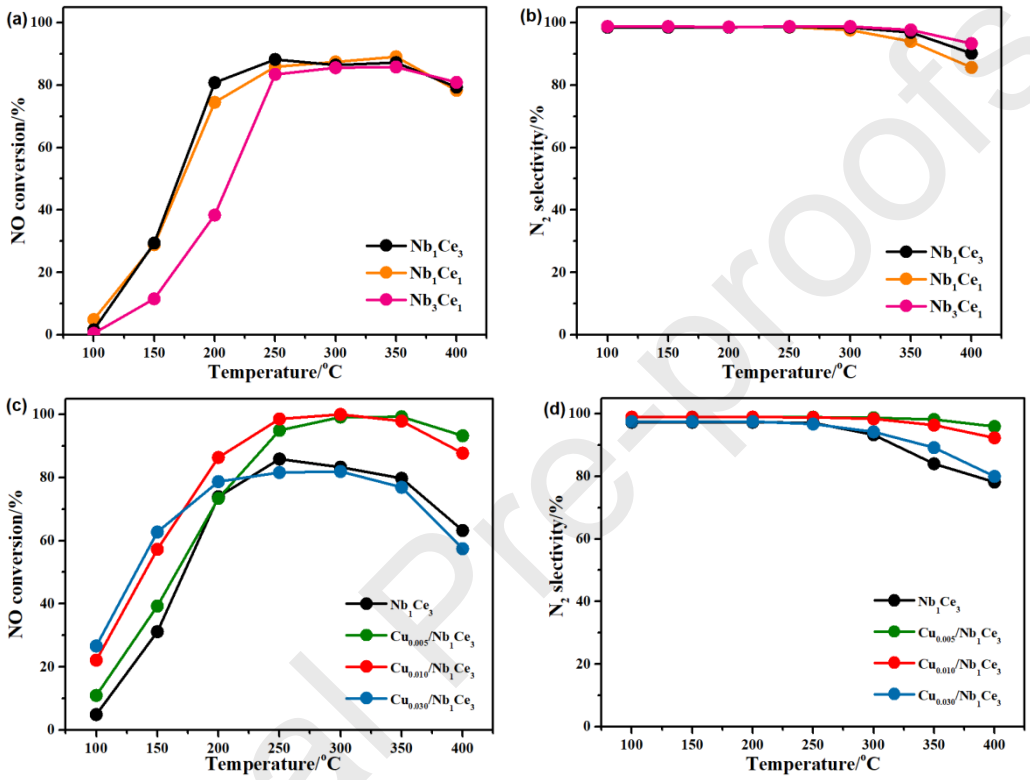

Fig. 1. NO conversion and N_2 selectivity of (a-b) NbCe and (c-d) Cu/Nb_1Ce_3 as a function of the reaction temperature. (The feeding gas contained 0.5‰ of NH_3, 0.5‰ of NO and 5 %(volume) O_2 balanced with Ar. Weight hourly space velocity (WHSV) = 60,000 $ml \cdot g^{-1} \cdot h^{-1}$.)

In the practical NH_3-SCR reaction, SO_2 and H_2O are considered as main deactivating species hence the excellent SO_2 and H_2O durability of catalyst is highly required [27]. As illustrated in Fig. 2, $Cu_{0.010}/Nb_1Ce_3$ and Nb_1Ce_3 were implemented to estimate the SO_2 and/or H_2O resistance. The SO_2 and H_2O durability test was conducted at 275 °C and the reaction was operated for 5 h before exposing to H_2O. The addition

of 5 %(volume) H_2O had a negligible inhibition effect on the SCR performance and the NO conversion restored to initial state once the H_2O supply was turned off, which indicated that the deactivation of H_2O was reversible. When 0.2‰ SO_2 was introduced into the feed for 7 h, the activity of $Cu_{0.010}/Nb_1Ce_3$ only declined from 100% to 95% in first one hour and then stabilized. However, the activity of Nb_1Ce_3 continued to drop from 85% to 75% until the SO_2 was cut off. Then both SO_2 and H_2O were introduced into the feed to examine the combined effect and the deNO_x efficiency of Nb_1Ce_3 exhibited sharply impaired. Its activity dropped from 80% to 45% within one hour, and then slowly recovered to 75% in the next 11 h. The corresponding NO conversion of $Cu_{0.010}/Nb_1Ce_3$ decreased to 90% after 12 h, and restored to almost 95% when the SO_2 and H_2O supply was turned off, suggesting the deactivated $Cu_{0.010}/Nb_1Ce_3$ catalyst was easy to regenerate. Thus, it could be concluded that the $Cu_{0.010}/Nb_1Ce_3$ catalyst still displayed outstanding NH_3-SCR of NO performance even in the presence of SO_2 and H_2O.

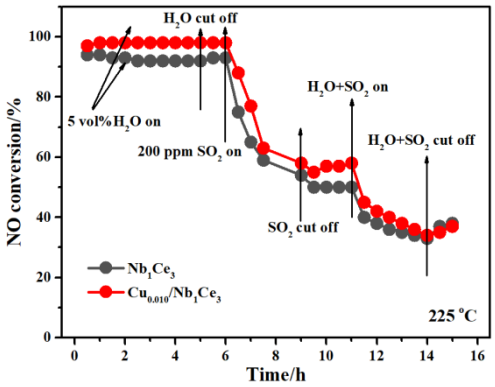

Fig. 2. Tolerance tests over Nb_1Ce_3 and $Cu_{0.010}/Nb_1Ce_3$ as a function of the reaction time. (The feeding gas contained 0.5‰ of NH_3, 0.5‰ of NO, 5 %(volume) O_2, 5 %(volume) H_2O (when used) and 0.2‰ of SO_2 (when used) balanced with Ar. Weight hourly space velocity (WHSV) =

60,000 ml·g^{-1}·h^{-1}.)

3.2 Physicochemical characterizations

The XRD patterns of the catalysts were presented in Fig. 3. All the catalysts provided typical diffraction peaks for the CeO_2 cubic phase (JCPDS 34-0394) and no diffraction peaks attributed to Nb species were detected, indicating that Nb species existed as amorphous. After Cu modification, the diffraction peaks of Cu/Nb_1Ce_3 catalysts were broader than Nb_1Ce_3 catalysts (clearer in the enlarged pattern attached to and FWHM obtained by fitting a Gaussian function) and no bands intensity ascribed to CuO were observed. This indicated that Cu ions inserted into the lattice of the Nb_1Ce_3 catalysts or was highly dispersed on the surface of Cu/Nb_1Ce_3 catalysts [28].

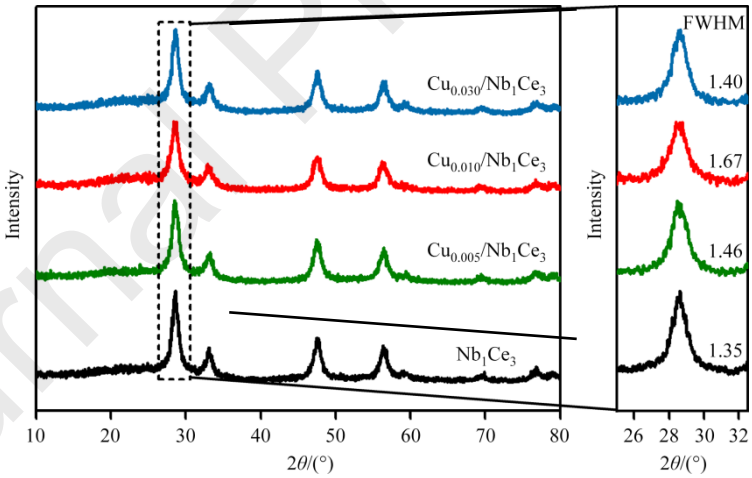

Fig. 3. XRD patterns of Nb_1Ce_3 and Cu/Nb_1Ce_3.

The actual molar ratio of Cu to Nb_1Ce_3 in the as prepared Cu/Nb_1Ce_3 samples were detected by XRF analysis and the results were listed in Table 1. And they were basically consistent with the theoretical value, which proved that our samples were successfully prepared.

The BET surface area, pore volume, and average pore size derived from N_2 physisorption results were shown in Table 1. It was noticeably that the S_{BET} of Cu/Nb_1Ce_3 catalysts gradually decreased with the increase of Cu addition yet its catalytic activities significantly preceded that of the Nb_1Ce_3 catalyst. This indicated that the SCR performance did not directly depend on the specific surface area in such catalyst system. In addition, the pore volume of all samples decreased from 0.10 to 0.08 $cm^{-3}\cdot g^{-1}$ while the pore size changed conversely with Cu modification. This manifested that the Cu species entered the pores of Nb_1Ce_3 and caused the plugging to a certain extent.

Table 1. Physicochemical properties of Nb_1Ce_3 and Cu/Nb_1Ce_3.

Samples	Cu actual ratio	$S_{BET}/m^2\cdot g^{-1}$	Pore volume/$cm^{-3}\cdot g^{-1}$	Pore size/nm
Nb_1Ce_3	-	66.5	0.12	3.49
$Cu_{0.005}/Nb_1Ce_3$	0.0067	49.3	0.10	2.88
$Cu_{0.010}/Nb_1Ce_3$	0.013	35.1	0.09	3.31
$Cu_{0.030}/Nb_1Ce_3$	0.033	28.4	0.08	3.41

Raman spectra were also collected to further explain the catalyst structure and depicted in Fig. 4. An intensive band centered at 463 cm^{-1} was observed on Nb_1Ce_3, which was attributed to the F_{2g} mode characteristic of the fluorite structure of ceria [29]. As for Cu/Nb_1Ce_3, the CuO bands were completely absent, illuminating the amorphous state of CuO species as the XRD patterns suggested. The band at 446 cm^{-1} ascribed to

F_{2g} showed an obvious shift toward lower wavenumber, signifying a decrease in the Ce-O bond order. This illustrated that the Cu-O-Ce solid solution may occur due to the Cu modification. In addition, two bands detected at 314 and 800 cm^{-1} were ascribed to the Nb_2O_5 phase [30], indicative of the existence of the Nb-O symmetric modes of the NbO_4 tetrahedral structure. NbO_4 was deemed as a highly active site, which was conducive to the adsorption and activation of NH_3 [19]. It should be noted that the intensity of NbO_4 tetrahedral coordination was the most obvious in $Cu_{0.010}/Nb_1Ce_3$ compared with other samples and this further corroborated the above activity test results. And the weakening of Ce-O bond and the appearance of NbO_4 indicated that there was a strong interaction among Cu, Nb and Ce species.

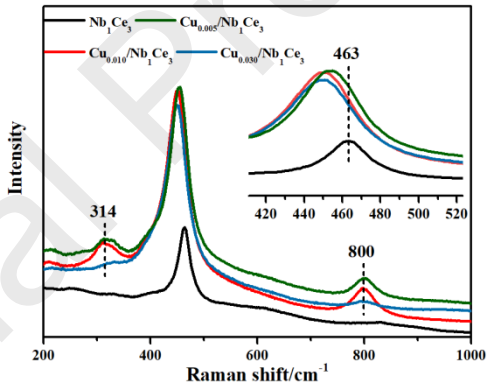

Fig. 4. Raman spectra of Nb_1Ce_3 and Cu/Nb_1Ce_3.

3.3 Surface elements properties

To better understand the surface chemical states of the catalysts, XPS measurements were conducted and the results were displayed in Fig. 5. Ce 3d, Nb 3d and O 1s were analyzed and the main surface metal content was summarized in Table 2.

Table 2. Surface atomic ratio of Nb_1Ce_3 and Cu/Nb_1Ce_3.

Samples	Cu atomic concentration /%(mass)	Surface atomic ratio/%		
		$Ce^{3+}/(Ce^{3+}+Ce^{4+})$	$O_\alpha/(O_\alpha+O_\beta)$	$Nb^{5+}/(Nb^{5+}+Nb^{4+})$
Nb_1Ce_3	-	26.4	37.3	73.7
$Cu_{0.005}/Nb_1Ce_3$	1.36	25.9	27.6	76.6
$Cu_{0.010}/Nb_1Ce_3$	2.20	27.8	33.1	83.6
$Cu_{0.030}/Nb_1Ce_3$	3.28	27.6	33.7	71.5

Due to the low Cu content, its peaks in XPS were greatly affected by the signal-to-noise ratio, so the atomic concentration was analyzed. As the Cu species addition increased, the concentration of Cu atoms on the surface of the catalyst gradually increased as well. However, it changed slowly (2.20% vs 3.28%) when the Cu loading exceeded 1 %(mass), which might be attributed to the occurrence of agglomerated Cu species. The agglomerated Cu species would lead to the oxidation of NH_3 [31], which explained the reason why the catalytic activity of the $Cu_{0.030}/Nb_1Ce_3$ catalyst degraded at high temperature.

The spectrum of Ce 3d was deconvoluted into ten peaks and the corresponding results were given in Fig. 5(a). The deconvoluted peaks labeled as "u" symbolized the Ce $3d_{3/2}$ spin-orbit components, and those donated as "v" symbolized the Ce $3d_{5/2}$ spin-orbit components. And the peak labeled as v_0, v′, u_0, and u′ were assigned to the Ce^{3+} species, peaks donated as v, v″, v‴, u, u″, and u‴ belonged to the Ce^{4+} species

[26]. $Cu_{0.010}/Nb_1Ce_3$ acquired the highest $Ce^{3+}/(Ce^{4+}+Ce^{3+})$ ratio compared with Nb_1Ce_3 and other Cu modified catalysts. A higher concentration of surface Ce^{3+} might be beneficial for the enhanced NH_3-SCR performance. It demonstrated that the addition of Cu effectively transformed the Ce^{4+} to Ce^{3+} on the surface of $Cu_{0.010}/Nb_1Ce_3$ through the interaction between Cu and Ce species [22].

Nb 3d spectra were presented in Fig. 5(b) and the binding energy of Nb $3d_{5/2}$ located at 206.8 and 205.6 eV could be ascribed to the Nb^{5+} and Nb^{4+} species, indicating that Nb species on Nb_1Ce_3 and $Cu_{0.010}/Nb_1Ce_3$ were mainly in the highest valence state [32]. Nb^{5+} was easier to enter the tetrahedral vacancy of oxygen due to its smaller radius than Nb^{4+} and thus the active NbO_4 species appeared. The proper content of Cu modification facilitated $Cu_{0.010}/Nb_1Ce_3$ to acquire the most $Nb^{5+}/(Nb^{5+}+Nb^{4+})$ ratio through the interaction between Cu and Nb.

As depicted in Fig. 5(c), the XPS spectra of O 1s were fitted into two peaks. The O 1s binding energy located at 530.4-531.1 eV was attributed to the chemisorbed oxygen species including O^- and O_2^- (donated as O_α) and the binding energy at 529.4.4-529.9 eV was ascribed to the lattice oxygen species (denoted as O_β) [33]. $Cu_{0.010}/Nb_1Ce_3$ acquired the highest $O_\alpha/(O_\alpha+O_\beta)$ ratio, demonstrating that the $Cu_{0.010}/Nb_1Ce_3$ catalyst possessed a large amount of the surface chemisorbed oxygen species, which was favor of NO oxidation to NO_2 [24]. Thus, the abundant amount of chemisorbed oxygen species on the surface of $Cu_{0.010}/Nb_1Ce_3$ could contribute to the fast-SCR reaction and consequently much better activity at low temperature.

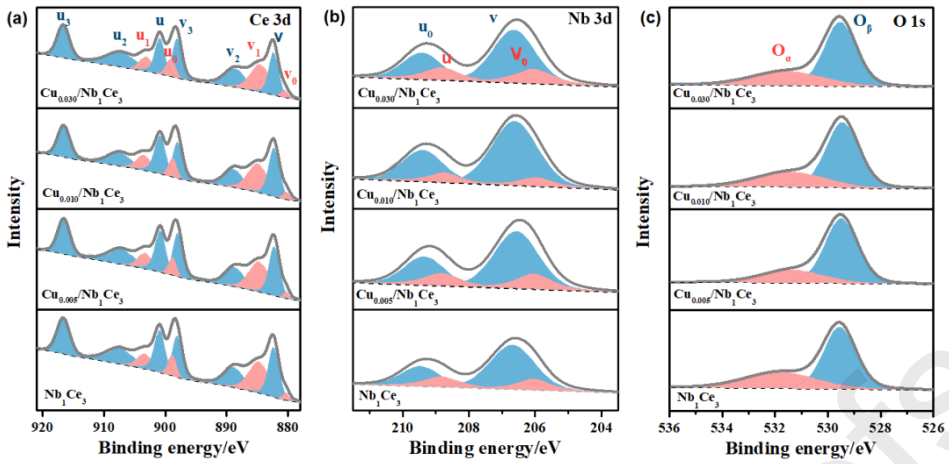

Fig. 5. XPS spectra of (a) Ce 3d, (b) Nb 3d and (c) O 1s for Nb_1Ce_3 and Cu/Nb_1Ce_3.

A deeper understanding towards the existence state of Cu species was obtained by EPR, shown in Fig. 6. Only Cu^{2+} species with d^9 electronic structure gave EPR signal, whereas other Cu valence were EPR silent [34]. The signal A was a typical peak of monomeric Cu^{2+} in octahedral sites with a tetragonal distortion [35]. The signal K at 3000 G was assigned to dimeric Cu^{2+} generated from the coupled unpaired electrons of two Cu^{2+} [36]. It's quite clear that both the $Cu_{0.010}/Nb_1Ce_3$ and $Cu_{0.030}/Nb_1Ce_3$ had much more monomeric Cu^{2+} species. Besides, the distinct K signal of $Cu_{0.030}/Nb_1Ce_3$ provided evidence for the excessive Cu addition induced agglomeration of Cu species.

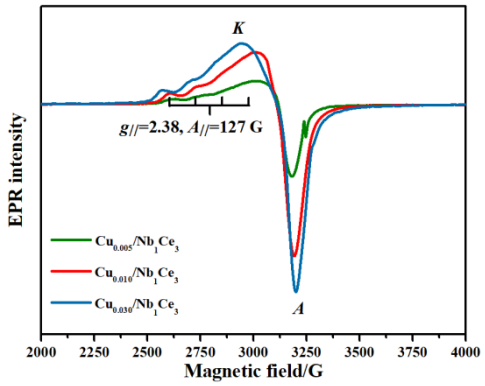

Fig. 6. EPR spectra of Nb_1Ce_3 and Cu/Nb_1Ce_3.

To further confirm the surface state and content of Cu species, *in situ* DRIFTS was

performed for NO chemisorption. The interaction of NO with Cu^{2+} and Cu^{+} would give specific bands, so it's a reasonable semi-quantitative means to determine the $Cu^{2+}/(Cu^{2+}+Cu^{+})$ ratio. Cu/Nb_1Ce_3 catalysts were exposed to flowing NO/N_2 until saturated at room temperature and the result was shown in Fig. 7. The band detected at *ca.*1905 cm^{-1} was ascribed to the Cu^{2+}-NO and *ca.*1847 cm^{-1} was ascribed to the Cu^{+}-NO [37]. Later, the peak area was integrated respectively and the $Cu^{2+}/(Cu^{2+}+Cu^{+})$ ratio was further calculated as placed in Table 3. Obviously, the $Cu_{0.010}/Nb_1Ce_3$ catalyst had the highest $Cu^{2+}/(Cu^{2+}+Cu^{+})$ ratio.

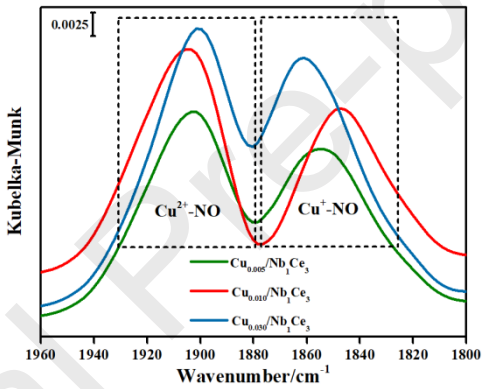

Fig. 7. *in situ* DRIFTS spectra of Cu/Nb_1Ce_3 saturated in NO at room temperature.

Table 3. Surface $Cu^{2+}/(Cu^{2+}+Cu^{+})$ ratio of Cu/Nb_1Ce_3 derived from NO-*in situ* DRIFTS

Samples	$Cu^{2+}/(Cu^{2+}+Cu^{+})$/%
$Cu_{0.005}/Nb_1Ce_3$	55.5
$Cu_{0.010}/Nb_1Ce_3$	58.9
$Cu_{0.030}/Nb_1Ce_3$	53.0

3.4 Clarification of Cu promoting mechanism

H_2-TPR was performed to reveal the promotional effect of Cu modification on the

redox properties of Nb_1Ce_3 and the results were reported in Fig. 8. A broad reduction peak occurred on the Nb_1Ce_3 surface from 400 °C to 750 °C, which could be associated with the reduction of the surface capping oxygen [20, 38]. For Cu/Nb_1Ce_3, a new reduction peak centered at about 200-300 °C occurred, representing that the Cu^{2+} was reduced to Cu^+ and then Cu^+ was converted to metallic Cu [39], suggesting the significant enhancement of redox ability in low-temperature range. It's observed that the reduction peak of Cu species shifted to lower temperature with the Cu addition increased, proving that the gradually enhanced redox properties of Cu/Nb_1Ce_3. Besides, the peak of surface capping oxygen moved to the lower temperature due to the interaction among Cu, Nb and Ce species. Nevertheless, excessive redox capacity would lead to the occurrence of NH_3-SCR side reactions at high temperature, resulting in diminishment for NO removal [31]. Therefore, it could be inferred that the strong redox property generated from agglomerated Cu species on $Cu_{0.030}/Nb_1Ce_3$ made the weakened denitration efficiency at high temperature [40]. However, an appropriate redox property generated from highly dispersed isolated Cu species enabled $Cu_{0.010}/Nb_1Ce_3$ to acquire a promoted SCR performance over a wide temperature.

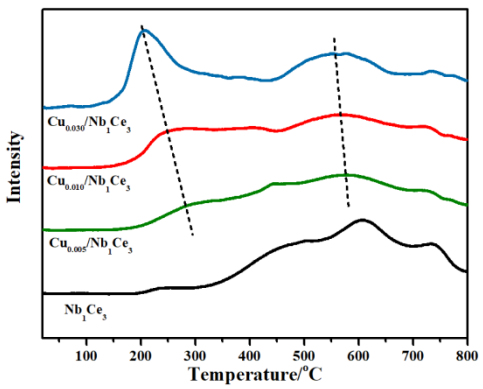

Fig. 8. H_2-TPR profiles of Nb_1Ce_3 and Cu/Nb_1Ce_3.

Cu modification efficaciously enhanced the denitration efficiency of Nb_1Ce_3 and the $Cu_{0.010}/Nb_1Ce_3$ catalyst with the most Cu^{2+} exhibited the best activity. Hence, the effect of Cu^{2+} on the denitrification reaction was worthy of further investigation. Recently studies showed that for Cu loaded zeolite catalysts, Cu^{2+} would induce the Cu^{2+}-NO_3^-+NO(g)→Cu^{2+}-NO_2^-+NO_2(g) reaction, then the generated NO_2 promoted fast-SCR reaction and improved low-temperature NH_3-SCR reaction [37]. Herein, an experiment of NO reduction of surface nitrates was conducted to explore the promotional effect of Cu^{2+}. NO+O_2/N_2 were pre-adsorbed on Cu/Nb_1Ce_3 catalysts until saturated at 150 °C so that nitrates were formed on the surface. Then the catalyst was exposed to the NO after purged in inert atmosphere and the NO_2 formation was recorded in Fig. 9. It could be clearly seen that the NO_2 formation increased after Cu modification and the promoting effect was volcanic with the increase of Cu^{2+} content. $Cu_{0.010}/Nb_1Ce_3$ catalyst with the most Cu^{2+} activated and reduced more surface nitrates to generate the most NO_2. This helped to reveal the promotional mechanism of Cu^{2+} on the low-temperature deNO_x performance of $Cu_{0.010}/Nb_1Ce_3$ catalyst.

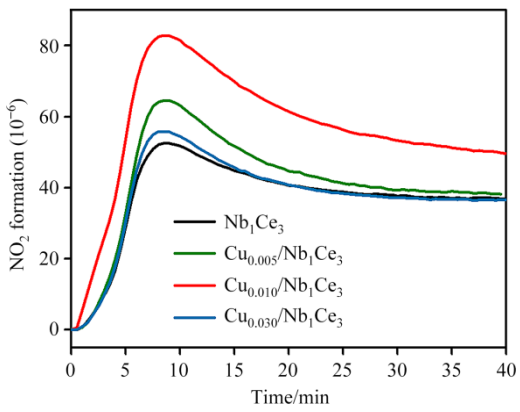

Fig. 9. NO_2 formation of Nb_1Ce_3 and Cu/Nb_1Ce_3.

It's known that a key step in the catalytic reaction was the desorption process of the product, so the NO_2 adsorption capacity was further evaluated by NO_2-TPD. As shown in Fig. 10, after Cu modification, the desorption temperature of ad-NO_2^- [41] over $Cu_{0.010}/Nb_1Ce_3$ catalyst decreased significantly, from 242 °C to 155 °C. The easier the NO_2 desorbed, the faster the SCR reaction carried out. Besides, the desorption peak at high temperature was related to the strongly adsorbed nitrates [42], their easy desorption would also be beneficial to more sites available for NH_3 adsorption. And the NO elimination at high temperature was further facilitated.

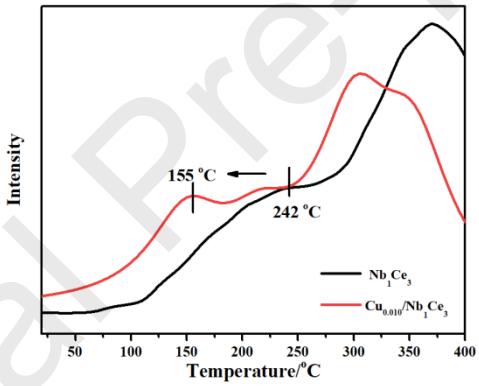

Fig. 10. NO_2-TPD profiles of Nb_1Ce_3 and $Cu_{0.010}/Nb_1Ce_3$.

3.5 Adsorption properties

Surface acidity was another decisive factor for the NH_3-SCR reaction. Therefore, NH_3-TPD was performed to determine the amount of acid sites and acid strength. As shown in Fig. 11, all samples showed a broad desorption peak in the range of 50−450 °C and the profiles changed little after Cu modification. The integrated peak areas manifested that the $Cu_{0.010}/Nb_1Ce_3$ catalyst showed the highest NH_3 adsorption capacity

among all Cu modified NbCe catalysts. And the decrease in total acid sites probably caused by the coverage of agglomerated Cu species.

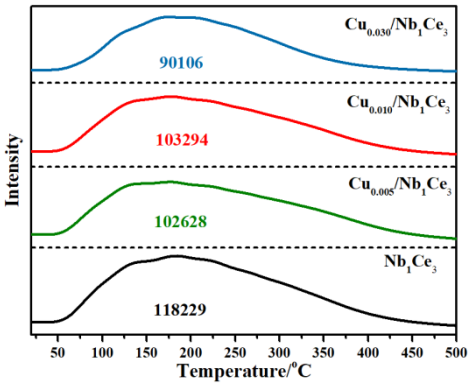

Fig. 11. NH_3-TPD profiles of Nb_1Ce_3 and Cu/Nb_1Ce_3.

To further distinguish the specific adsorption sites of NH_3, Fig. 12 illustrated the results of *in situ* DRIFTS spectra of NH_3-TPD over (a) Nb_1Ce_3 and (b) $Cu_{0.010}/Nb_1Ce_3$. For Nb_1Ce_3 catalyst, the bands centered at *ca.* 1604, 1568, 1297 and 1190 cm^{-1} could be ascribed to bending vibrations of N-H bonds in NH_3 coordinately linked to Lewis acid sites [43, 44], while the weak band at *ca.* 1612 and 1458 cm^{-1} was assigned to bending vibrations of ionic NH_4^+ on the Brønsted acid sites [6, 38]. For $Cu_{0.010}/Nb_1Ce_3$ catalyst, bands ascribed to Brønsted acid sites were distinctly enhanced on account of the Cu modification. This should be caused by the appearance of NbO_4 species due to the strong interaction between Nb and Cu species as Raman spectra indicated [26].

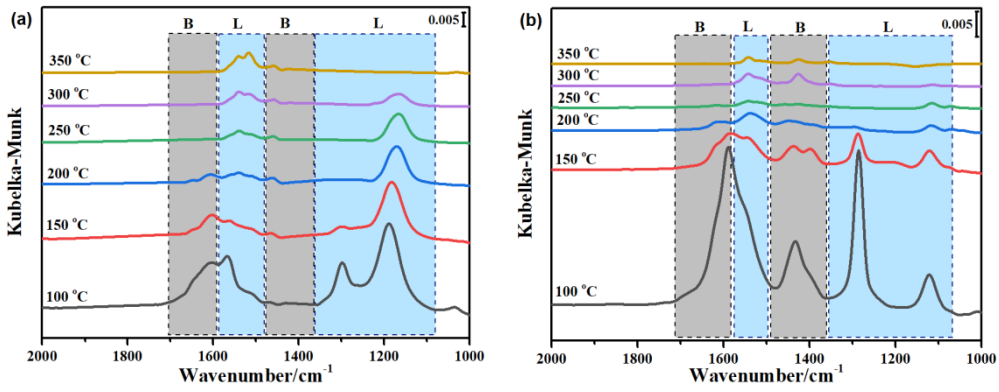

Fig. 12. *in situ* DRIFTS spectra of (a) Nb_1Ce_3 and (b) $Cu_{0.010}/Nb_1Ce_3$ saturated in NH_3 at 100 °C and then purged by N_2 from 100 °C to 350 °C.

The $NO+O_2$-TPD over (a) Nb_1Ce_3 and (b) $Cu_{0.010}/Nb_1Ce_3$ were also carried out through *in situ* DRIFTS. As depicted in Fig. 13, the bands of bridging bidentate nitrates (1625, 1607 and 1208 cm^{-1}), chelating bidentate nitrates (1580, 1540 and 1238 cm^{-1}), monodentate nitrates (1548 cm^{-1}) and *cis*-$(N_2O_2)^{2-}$ (1026 and 1000 cm^{-1}) were observed [38, 44]. It could be found that after Cu modification, the ad-nitrate species were almost unchanged, but the thermal stability of the nitrates on $Cu_{0.010}/Nb_1Ce_3$ catalyst was remarkably reduced. This manifested that the nitrates adsorbed on $Cu_{0.010}/Nb_1Ce_3$ was more easily activated to participate in the following reaction, and thus the adsorption and activation sites would be more accessible for NH_3 at higher temperature.

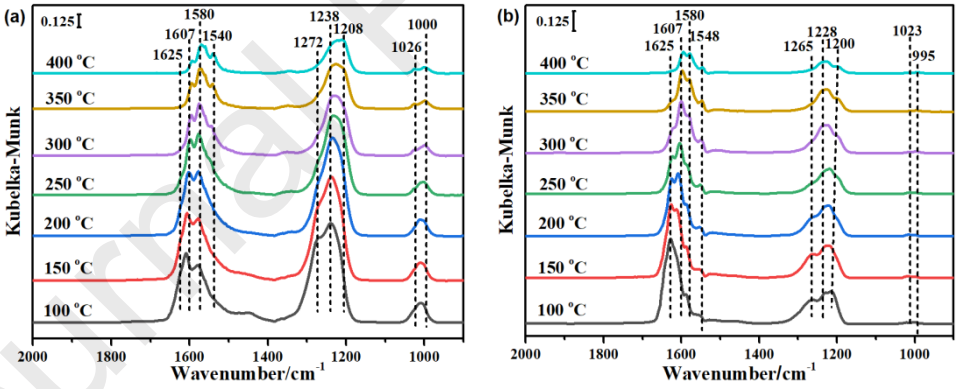

Fig. 13. *in situ* DRIFTS spectra of (a) Nb_1Ce_3 and (b) $Cu_{0.010}/Nb_1Ce_3$ saturated in $NO+O_2$ at 100 °C and then purged by N_2 from 100 °C to 350 °C.

3.6 Reaction mechanism

To determine the reactivity of NH_3 on $Cu_{0.010}/Nb_1Ce_3$, *in situ* DRIFTS was conducted at 150 °C with a flowing stream of $NO+O_2$ reacting with preadsorbed NH_3

(Fig. 14(a)). Upon introducing NO+O_2 to catalyst preadsorbed with NH_3, the bands assigned to NH_3 on Lewis and Brønsted acid sites consumed rapidly, suggesting that the SCR reaction on $Cu_{0.010}/Nb_1Ce_3$ could proceed through the Eley-Rideal (E − R) mechanism efficiently. In turn, the reactivity of adsorbed nitrates on $Cu_{0.010}/Nb_1Ce_3$ was also studied with NH_3 reacting with preadsorbed NO+O_2 (Fig. 14(b)). The bands assigned to nitrate species (bridged nitrate at 1621 cm^{-1}, monodentate nitrates at 1539, 1442 and 1290 cm^{-1}) were displayed. Afterwards, NH_3 were introduced, the intensity of bridge nitrate was weakened and the monodentate nitrate was reconstructed, indicating that the adsorbed nitrates could not react with NH_3. Therefore, the SCR reaction followed Eley-Rideal (E-R) mechanism over $Cu_{0.010}/Nb_1Ce_3$ at 150 °C.

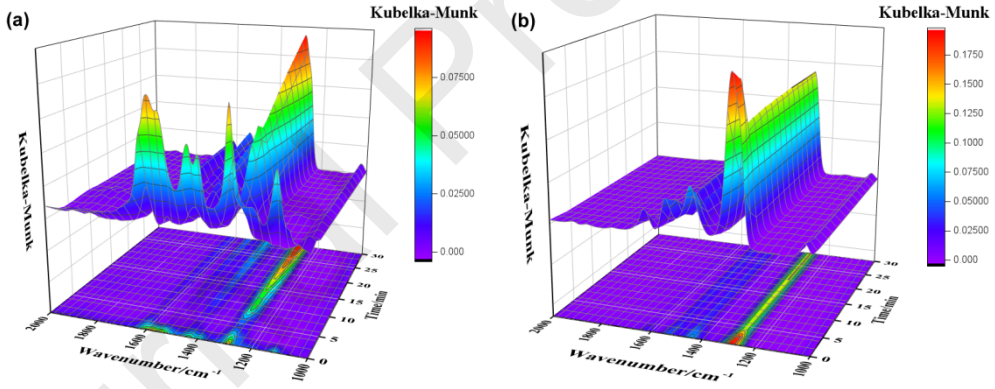

Fig. 14. *in situ* DRIFTS spectra of NH_3-SCR reaction on $Cu_{0.010}/Nb_1Ce_3$ at 150 °C.

4. Conclusions

A series of Cu modified NbCe catalysts were prepared and applied in the NH_3-SCR process. The ternary oxides catalysts presented promising NO conversion in a broad reaction temperature window compared with binary oxides NbCe catalyst. Among all the synthesized catalysts, the $Cu_{0.010}/Nb_1Ce_3$ catalyst showed the optimal

NO abatement efficiency from 200 to 400 °C, together with near 100% N_2 selectivity. Besides, H_2O or/and SO_2 had a slightly reversible inhibition influence on the catalytic activity. Several conclusions can be drawn through an array of characterization: The proper amount of Cu modification made the active Cu species highly dispersed in the form of monomeric or dimeric Cu^{2+} on $Cu_{0.010}/Nb_1Ce_3$, facilitating the less stable nitrates, the formation/desorption of NO_2 and the fast-SCR reaction. Meanwhile, the interaction between Cu and Nb species induced the generation of highly active NbO_4 species and more surface acid sites, therefore the adsorption and activation of NH_3 were enhanced, which were all responsible for the excellent NH_3-SCR activity. Nevertheless, excessive Cu addition would lead to the appearance of agglomerated Cu species, resulting in undesirable NH_3 oxidation and eventually impaired deNO_x efficiency at high temperature.

Declaration of Competing Interest

The authors declare that they have no known competing financial interests or personal relationships that could have appeared to influence the work reported in this paper.

Acknowledgements

Financial support from the National Natural Science Foundation of China (No. 21972062, 21976081, 21976111) is gratefully acknowledged.

References

[1] M. Barreau, M.L. Tarot, D. Duprez, X. Courtois, F. Can, Remarkable enhancement of the

selective catalytic reduction of NO at low temperature by collaborative effect of ethanol and NH_3 over silver supported catalyst, *Appl. Catal. B: Environ.*, 220 (2018) 19-30.

[2] Z. Ma, X. Wu, H. Härelind, D. Weng, B. Wang, Z. Si, NH_3-SCR reaction mechanisms of $NbO_x/Ce_{0.75}Zr_{0.25}O_2$ catalyst: DRIFTS and kinetics studies, *J. Mol. Catal. A: Chem.*, 423 (2016) 172-180.

[3] T. Zhang, R. Qu, W. Su, J. Li, A novel Ce-Ta mixed oxide catalyst for the selective catalytic reduction of NO_x with NH_3, *Appl. Catal. B: Environ.*, 176-177 (2015) 338-346.

[4] M.F. Irfan, J.H. Goo, S.D. Kim, Co_3O_4 based catalysts for NO oxidation and NO_x reduction in fast SCR process, *Appl. Catal. B: Environ.*, 78 (2008) 267-274.

[5] S. Roy, M.S. Hegde, G. Madras, Catalysis for NO_x abatement, *Appl. Energy*, 86 (2009) 2283-2297.

[6] S. Ding, F. Liu, X. Shi, H. He, Promotional effect of Nb additive on the activity and hydrothermal stability for the selective catalytic reduction of NO_x with NH_3 over $CeZrO_x$ catalyst, *Appl. Catal. B: Environ.*, 180 (2016) 766-774.

[7] F. Liu, H. He, Y. Ding, C. Zhang, Effect of manganese substitution on the structure and activity of iron titanate catalyst for the selective catalytic reduction of NO with NH_3, *Appl. Catal. B: Environ.*, 93 (2009) 194-204.

[8] J.P. Dunn, P.R. Koppula, H. G. Stenger, I.E. Wachs, Oxidation of sulfur dioxide to sulfur trioxide over supported vanadia catalysts, *Appl. Catal. B: Environ.*, 19 (1998) 103-117.

[9] P. Li, Y. Xin, Q. Li, Z. Wang, Z. Zhang, L. Zheng, Ce-Ti amorphous oxides for selective catalytic reduction of NO with NH_3: Confirmation of Ce-O-Ti active sites, *Environ. Sci. & Technol.*, 46 (2012) 9600-9605.

[10] G. Busca, L. Lietti, G. Ramis, F. Berti, Chemical and mechanistic aspects of the selective catalytic reduction of NO_x by ammonia over oxide catalysts: A review, *Appl. Catal. B: Environ.*, 18 (1998) 1-36.

[11] M. Stanciulescu, G. Caravaggio, A. Dobri, J. Moir, R. Burich, J.P. Charland, P. Bulsink, Low-temperature selective catalytic reduction of NO_x with NH_3 over Mn-containing catalysts, *Appl. Catal. B: Environ.*, 123-124 (2012) 229-240.

[12] J.W. Ji, Y. Tang, L. Han, P. Ran, W. Song, Y.D. Cai, W. Tan, J.F. Sun, C.J. Tang, L. Dong, Cerium manganese oxides coupled with ZSM-5: A novel SCR catalyst with superior K resistance, *Chem. Eng. J*, (2022) 136530.

[13] L. Chen, Z. Si, X. Wu, D. Weng, DRIFT study of $CuO-CeO_2-TiO_2$ mixed oxides for NO_x reduction with NH_3 at low temperatures, *ACS Appl. Mater. & Inter.*, 6 (2014) 8134-8145.

[14] C. Tang, H. Zhang, L. Dong, Ceria-based catalysts for low-temperature selective catalytic reduction of NO with NH_3, *Catal. Sci. & Technol.*, 6 (2016) 1248-1264.

[15] N.-Y. Topsøe, Mechanism of the selective catalytic reduction of nitric oxide by ammonia elucidated by in situ on-line fourier transform infrared spectroscopy, *Science*, 265 (1994) 1217-1219.

[16] H.D. Xu, J.X. Liu, Z.H. Zhang, S. Liu, Q.J. Lin, Y. Wang, S. Dai, Y.Q. Chen, Design and synthesis of highly-dispersed WO_3 catalyst with highly effective NH_3-SCR activity for NO_x abatement, *ACS Catal.*, 9 (2019) 11557-11562.

[17] S. Liu, P. Yao, Q.J. Lin, S.H. Xu, M.M. Pei, J.L. Wang, H.D. Xu, Y.Q. Chen, Optimizing acid

promoters of Ce-based NH_3-SCR catalysts for reducing NO_x emissions, *Catal. Today.*, 382 (2021) 34-41.

[18] S. Liu, P. Yao, M.M. Pei, Q.J. Lin, S.H. Xu, J.L. Wang, H.D. Xu, Y.Q. Chen, Significant differences of NH_3-SCR performances between monoclinic and hexagonal WO_3 on Ce-based catalysts, *Environ. Sci.: Nano.*, 8 (2021) 2988-3000.

[19] R. Qu, X. Gao, K. Cen, J.J.A.C.B.E. Li, Relationship between structure and performance of a novel cerium-niobium binary oxide catalyst for selective catalytic reduction of NO with NH_3, *Appl. Catal. B: Environ.*, 142 (2013) 290-297.

[20] W. Tan, C. Wang, S. Yu, Y. Li, S. Xie, F. Gao, L. Dong, F. Liu, Revealing the effect of paired redox-acid sites on metal oxide catalysts for efficient NO_x removal by NH_3-SCR, *J. Hazard. Mater.*, 416 (2021) 125826.

[21] L. Qi, Q. Yu, Y. Dai, C. Tang, L. Liu, H. Zhang, F. Gao, L. Dong, Y. Chen, Influence of cerium precursors on the structure and reducibility of mesoporous CuO-CeO_2 catalysts for CO oxidation, *Appl. Catal. B: Environ.*, 119-120 (2012) 308-320.

[22] Z. Wang, Z. Qu, X. Quan, Z. Li, H. Wang, R. Fan, Selective catalytic oxidation of ammonia to nitrogen over CuO-CeO_2 mixed oxides prepared by surfactant-templated method, *Appl. Catal. B: Environ.*, 134-135 (2013) 153-166.

[23] L. Kundakovic, M. Flytzani-Stephanopoulos, Cu- and Ag-modified cerium oxide catalysts for methane oxidation, *J. Catal.*, 179 (1998) 203-221.

[24] S. Ali, L. Chen, Z. Li, T. Zhang, R. Li, S. Bakhtiar, X. Leng, F. Yuan, X. Niu, Y.J.A.C.B.E. Zhu, Cu_x-$Nb_{1.1-x}$ (x= 0.45, 0.35, 0.25, 0.15) bimetal oxides catalysts for the low temperature selective catalytic reduction of NO with NH_3, *Appl. Catal. B: Environ.*, 236 (2018) 25-35.

[25] X.X. Wang, Y. Shi, S.J. Li, W. Li, Promotional synergistic effect of Cu and Nb doping on a novel Cu/Ti-Nb ternary oxide catalyst for the selective catalytic reduction of NO_x with NH_3, *Appl. Catal. B: Environ.*, 220 (2018) 234-250.

[26] S. Xie, W. Tan, Y. Li, L. Ma, S.N. Ehrlich, J. Deng, P. Xu, F. Gao, L. Dong, F. Liu, Copper single atom-triggered niobia-ceria catalyst for efficient low-temperature reduction of nitrogen oxides, *ACS Catal.*, 12 (2022) 2441-2453.

[27] Y. Wang, W. Yi, J. Yu, J. Zeng, H. Chang, Novel methods for assessing the SO_2 poisoning effect and thermal regeneration possibility of MO_x-WO_3/TiO_2 (M = Fe, Mn, Cu, and V) catalysts for NH_3-SCR, *Environ. Sci. & Technol.*, 54 (2020) 12612-12620.

[28] X. Yao, L. Zhang, L. Li, L. Liu, Y. Cao, X. Dong, F. Gao, Y. Deng, C. Tang, Z. Chen, L. Dong, Y. Chen, Investigation of the structure, acidity, and catalytic performance of CuO/$Ti_{0.95}Ce_{0.05}O_2$ catalyst for the selective catalytic reduction of NO by NH_3 at low temperature, *Appl. Catal. B: Environ.*, 150-151 (2014) 315-329.

[29] A. Martínez-Arias, M. Fernández-García, L.N. Salamanca, R.X. Valenzuela, J.C. Conesa, J. Soria, Structural and redox properties of ceria in alumina-supported ceria catalyst supports, *J. Phys. Chem. B*, 104 (2000) 4038-4046.

[30] G. Zhang, Z. Yan, Three-component nonlinear Schrödinger equations: Modulational instability, Nth-order vector rational and semi-rational rogue waves, and dynamics, *Commun. Nonlinear Sci. Numer. Simul.*, 62 (2018) 117-133.

[31] J.H. Kwak, R.G. Tonkyn, D.N. Tran, D. Mei, J.J.A.C. Szanyi, Size-dependent catalytic

performance of CuO on gamma-Al_2O_3: NO reduction versus NH_3 oxidation, *ACS Catal.*, 2 (2015) 1432-1440.

[32] W. Tan, C. Wang, S. Yu, Y. Li, F.J.J.o.H.M. Liu, Revealing the effect of paired redox-acid sites on metal oxide catalysts for efficient NO removal by NH_3-SCR, *J. Hazard. Mater.*, 416 (2021) 125826.

[33] Z.R. Ma, X.D. Wu, Z.C. Si, D.Weng, J. Ma, Impacts of niobia loading on active sites and surface acidity in NbO_x/CeO_2-ZrO_2 NH_3-SCR catalysts, *Appl. Catal. B: Environ.*, 179 (2015) 380-394.

[34] Z. Chen, C. Fan, L. Pang, S. Ming, P. Liu, T. Li, The influence of phosphorus on the catalytic properties, durability, sulfur resistance and kinetics of Cu-SSZ-13 for NO_x reduction by NH_3-SCR, *Appl. Catal. B: Environ.*, 237 (2018) 116-127.

[35] A. Aboukais, A. Bennani, C.F. Aissi, M. Guelton, J.C. Vedrine, Microwave frequency behavior of the EPR copper(II) ion pairs spectrum formed in CuCe oxide, Chemistry of Materials, 4 (1992) 977-979.

[36] Y. Xiong, L. Li, L. Zhang, Y. Cao, S. Yu, C. Tang, L. Dong, Migration of copper species in $Ce_xCu_{1-x}O_2$ catalyst driven by thermal treatment and the effect on CO oxidation, *Phys. Chem. Chem. Phys.*, 19 (2017) 21840-21847.

[37] Y. Li, J. Deng, W. Song, J. Liu, Z. Zhao, M. Gao, Y. Wei, L. Zhao, Nature of Cu species in Cu-SAPO-18 catalyst for NH_3-SCR: Combination of experiments and DFT calculations, *J. Phys. Chem. C*, 120 (2016) 14669-14680.

[38] W. Tan, J. Wang, L. Li, A. Liu, G. Song, K. Guo, Y. Luo, F. Liu, F. Gao, L. Dong, Gas phase sulfation of ceria-zirconia solid solutions for generating highly efficient and SO_2 resistant NH_3-SCR catalysts for NO removal, *J. Hazard. Mater.*, 388 (2020) 121729.

[39] W.W. Wang, W.Z. Yu, P.P. Du, H. Xu, Z. Jin, R. Si, C. Ma, S. Shi, C.J. Jia, C.H. Yan, Crystal plane effect of ceria on supported copper oxide cluster catalyst for CO oxidation: Importance of metal-support interaction, *ACS Catal.*, 7 (2017) 1313-1329.

[40] Q.J. Lin, S. Liu, S.H. Xu, S. Xu, M.M. Pei, P. Yao, H.D. Xu, Y. Dan, Y.Q. Chen, Comprehensive effect of tuning Cu/SAPO-34 crystals using PEG on the enhanced hydrothermal stability for NH_3-SCR. *Catal. Sci. Technol.*, 11 (2021) 7640-7651.

[41] L. Chen, J. Li, M. Ge, R. Zhu, Enhanced activity of tungsten modified CeO_2/TiO_2 for selective catalytic reduction of NO_x with ammonia, *Catal. Today*, 153 (2010) 77-83.

[42] T. Gu, R. Jin, Y. Liu, H. Liu, X. Weng, Z. Wu, Promoting effect of calcium doping on the performances of MnO_x/TiO_2 catalysts for NO reduction with NH_3 at low temperature, *Appl. Catal. B: Environ.*, 129 (2013) 30-38.

[43] L. Li, L. Zhang, K. Ma, W. Zou, Y. Cao, Y. Xiong, C. Tang, L. Dong, Ultra-low loading of copper modified TiO_2/CeO_2 catalysts for low-temperature selective catalytic reduction of NO by NH_3, *Appl. Catal. B: Environ.*, 207 (2017) 366-375.

[44] X. Yao, R. Zhao, L. Chen, J. Du, C. Tao, F. Yang, L. Dong, Selective catalytic reduction of NO_x by NH_3 over CeO_2 supported on TiO_2: Comparison of anatase, brookite, and rutile, *Appl. Catal. B: Environ.*, 208 (2017) 82-93.

Declaration of Competing Interest

The authors declare that they have no known competing financial interests or personal relationships that could have appeared to influence the work reported in this paper.